Correlation between microstructure and mechanical properties of Al-Si diecast engine blocks

[1]Fabio Grosselle, [1]Giulio Timelli, [1]Franco Bonollo, [2]Roberto Molina
[1]Department of Management and Engineering, DTG, University of Padova, Vicenza, Italy
[2]Teksid Aluminum, Carmagnola, Italy

ABSTRACT

In spite of weight reduction of passenger car, the cylinder block is the heaviest component among many automotive engine parts and plays a key role in fuel efficiency and the drivability of vehicles. In hypoeutectic aluminium alloys, the final mechanical properties are strictly connected to microstructural features such as the distribution, the morphology and dimensions of primary α-Al phase and eutectic Si particles, as well as, type of iron-bearings and defects. The microstructure, in turn, depends on filling process and solidification dynamic. In this work, a HPDC 4-cylinders-in-line cylinder block was exhaustively analysed and mechanical properties were correlated to microstructural features. Mechanical properties are affected by microstructure. The best values of UTS and elongation to fracture are obtained for low secondary dendrite arm spacing (SDAS) values and small and more compact eutectic Si particles. If the combined effect of α-Al phase and eutectic Si particles is taken into account, a linear correlation between UTS and product of SDAS, equivalent diameter and aspect ratio of Si particles is observed, while the elongation to fracture shows an exponential trend, suggesting an high sensitivity on microstructural variation.

RIASSUNTO

Nel presente lavoro è stata analizzata la correlazione tra microstruttura e proprietà meccaniche di un blocco-motore 4 cilindri in linea pressocolato in lega di alluminio. Le proprietà meccaniche sono fortemente influenzate dalle caratteristiche microstrutturali della lega, quali la distribuzione e le dimensioni della fase α-Al e delle particelle di Si eutettico, la presenza di intermetallici ricchi in Fe o di eventuali difetti. La microstruttura dipende, a sua volta, dalla modalità di riempimento dello stampo e dalla velocità di solidificazione. I valori più elevati di UTS e di allungamento a rottura sono stati ottenuti in zone del getto caratterizzate da una microstruttura fine, ovvero, per bassi valori di spaziatura dendritica secondaria (SDAS) e particelle di Si eutettico piccole e compatte. L'elaborazione statistica dei dati sperimentali ha evidenziato una correlazione di tipo lineare tra UTS e il prodotto tra SDAS, diametro equivalente e rapporto d'aspetto delle particelle di Si eutettico, mentre una funzione di tipo esponenziale ha descritto la variazione dell'allungamento a rottura, mostrando un'alta sensibilità di tale proprietà alle caratteristiche microstrutturali.

KEYWORDS

Aluminium alloys; EN-AC 46000; High-pressure die-casting; SDAS; Eutectic Si; Microstructure; Engine block

INTRODUCTION

Aluminium alloy castings are making a significant contribution in the construction of modern passenger cars due to the potential capability in weight and emission reduction. In particular, the application of aluminium alloys to cylinder block, which is the main contributor to engine mass, in replacement of cast-iron offers very good potential to weigh reduction, up to 45% for gasoline engines. The enhancement in power rating owing to the highest thermal conductivity of aluminium alloys, three times better than that of cast iron, allows engines to deliver more power per cylinder size [1] due to a better control of local temperatures.

For mass produced engines, high-pressure die-casting (HPDC) is widely used for the

possibility of obtaining net to shape components of complex geometry and thin wall thickness at high production rates, reducing production costs [2-4]. Due to the complexity of the casting shape and variability in process parameters, common defects in industrial HPDC manufactured parts are shrinkage cavities, cold fills, oxide films, dross, entrapped air bubbles [4].

Due to excellent castability along with good mechanical properties achievable and low cost, hypoeutectic secondary Al-Si alloys are normally used for HPDC process. The microstructure expected in components cast with these alloys will be a mixture of pro-eutectic α-Al dendrites surrounded by Al–Si eutectic. The distribution, the morphology and dimension of primary α-Al and eutectic Si particles depend on cooling conditions and solidification history [5-8]. Moving from the wall in contact with the die to the centre line a very fine porosity-free microstructure becomes coarser and defects can easily form as consequence of filling dynamics and high solidification time [9]. The presence of Cu, Mg and tramp elements promotes the formation of other phases [1,10]. Copper and Magnesium lead to the formation of strengthening Al_2Cu and Mg_2Si precipitates [1-11] while iron promotes the formation of various intermetallic phases, the most common of which are needle-like β-Al_5FeSi and angular globules block-like $Al_{15}(Mn,Fe)_3Si_2$ [1-12].

Process parameters, microstructure features and defects contribute to the final mechanical properties of the aluminium alloy. In defect free components, fracture is initiated by cleavage of either brittle intermetallic or eutectic Si particles. Then, fracture propagates mainly along grain boundaries (intergranular mode) for small values of SDAS or along cell boundaries (transgranular mode) for large SDAS [13-15]. However, in presence of defects, mechanical properties decrease monotonically with an increase in the area fraction of defects as consequence of effect on fracture initiation and propagation [4,16-17].

In this work a HPDC engine block was analysed and mechanical properties were correlated to microstructural features, such as SDAS and the size and the morphology of eutectic Si particles. The material was an EN AC-46000–UNI EN 1706 alloy (European designation, equivalent to the US designation A380), widely used in load-bearing components in automotive field.

EXPERIMENTAL METHODS

In the present work, a secondary $AlSi_9Cu_3$ foundry alloy has been used. The chemical composition, measured on separately poured samples, is shown in Table I. The liquidus temperature of the alloy was determined by means of thermal analysis, T_{liq} = 585°C.

The Fe content was kept above 0.8 wt.%, to prevent the molten metal from "soldering" to the casting die. The Al–Si–Fe eutectic composition occurs at about 0.8 wt.% Fe. When Fe is alloyed to somewhat above this level, the molten metal has little or no tendency to dissolve die steel while the two materials are in intimate contact. Thus, the higher iron content of the alloy reduces the solution potential for the iron components of the casting machine and die, and for this reason, most aluminium pressure die casters desire that their alloys contain between 0.8 and 1.1 wt.% iron [18-20]. Further, the morphology of iron-rich β-phase, Al_5FeSi, deteriorates the strength and ductility behaviour of the alloy and promotes the initiation of cracks under load [21]. The addition of Manganese and the high solidification rate in die-casting change the morphology of Fe-bearing needles or enhance the precipitation of phases which are less harmful than β-phase. Manganese is also used to provide good ejection behaviour and reduced die soldering [22]. Magnesium, Copper and Zinc determine here the yield strength (YS) and the ultimate tensile strength (UTS).

The castings studied were HPDC 4-cylinders-in-line (L4) cylinder blocks. Figure 1 shows the open-deck geometry of the cylinder block and the location of the gates, runners and overflows. The castings were produced using a cold chamber die-casting machine equipped with the dynamic shot control system and the vacuum system connected to the venting channels. The engine blocks were cast with grey iron liners that resist the attrition of the

Table I. Chemical composition of the AlSi9Cu3 alloy studied in the present work (wt.%).

Alloy	Al	Si	Cu	Fe	Mg	Mn	Ni	Ti	Zn	Cr
EN-AC 46000	bal.	9.2	3.3	0.89	0.19	0.24	0.06	0.037	0.97	0.031

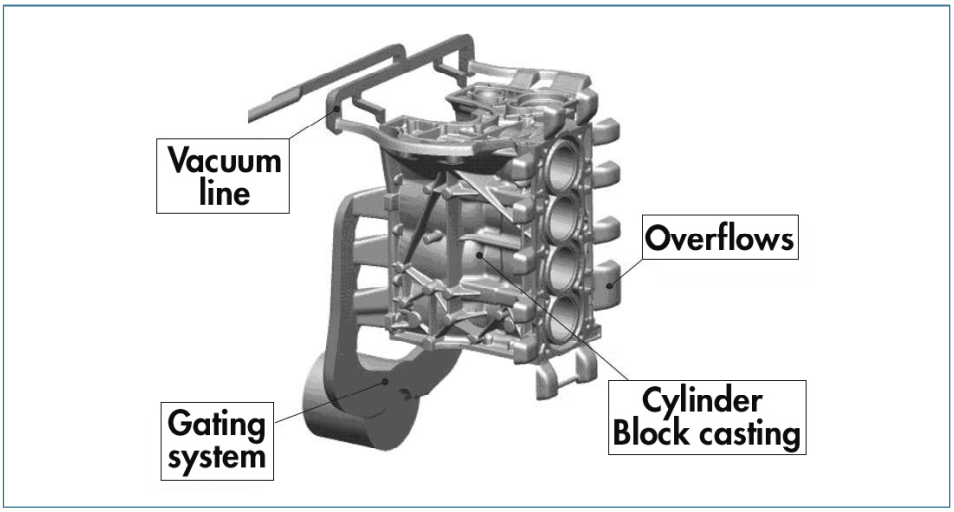

Fig. 1: Illustration of engine block with 6 ingates and the vacuum channels.

moving pistons. Each tubular liner was positioned directly into the die before pouring, remaining as cast-in inserts into the block. The melt was kept at ~690±10°C in the holding furnace and was automatically ladled into the shoot sleeve and injected into the die cavity. Several castings were scrapped after the startup, to reach a quasi-steady-state temperature in the shot chamber and die. Oil circulation channels in the die served to stabilize the temperature. The other best machine parameters including die temperature, injection speed of the melt and lubricant were selected to enable the mass production of the cylinder blocks. By means of a dynamic shot control system in the HPDC machine, every casting was documented with its shot profile, to monitor the final quality and repeatability.

Radiographic inspection was carried out throughout the castings, in order to detect the presence of macrodefects. The diecast engines were then sectioned and several blocks were drawn from different locations of the castings (Figure 2). Flat tensile test bars with rectangular cross section were machined from each of the blocks. The tensile specimens were 100 mm long, 20 mm wide, and 3 mm thick, with a gage length of 30 mm and a width of 10 mm, according to ASTM-B577.

The tensile tests were done on a computer controlled tensile testing machine MTS 810. The crosshead speed used was 2 mm/min (strain rate ~10^{-3} s^{-1}). The strain was measured using a 25-mm extensometer. Experimental data were collected and processed to provide yield stress (YS, actually 0.2% proof stress), ultimate tensile strength (UTS) and elongation to fracture (S_f). At least three specimens were tested for each zone. When the experimental data differed by more than 5%, another tensile specimen was tested. For the analysis in this paper, the average of the best values were selected in an attempt to minimise any effects arising from casting defects on the fracture data and to maximise the possibility of isolating the effects of microstructural parameters, such as SDAS and eutectic Si parameters. Contrary, casting defects do not generally affect YS values in the same way [16].

Microhardness measurements were performed on ground and polished samples cut from the gage sections of flat test bars. Vickers microhardness measurements were carried out using loads of 0.2 kgf and a 30-second dwell period, according to the standard ASTM E-384. The measurements were done at eight different locations along the cross section of the sample; the typical standard deviation was 5 HV.

The samples cut from the cross section of the gage length were mechanically prepared to a 1-μm finish with diamond paste and, finally, polished with a commercial fine silica slurry for metallographic investigations. Microstructural analysis was carried out using an optical microscope and a scanning electron microscope (SEM) equipped with an energy-dispersive spectrometer (EDS), and quantitatively analyzed using an image analyzer. To quantify the microstructural features, the image analysis was focused on the secondary dendrite arm spacing (SDAS), and on the size and aspect ratio of the eutectic silicon particles. Size is defined as the equivalent circle diameter (d); the aspect ratio (α) is the ratio of the maximum to the minimum Ferets. To obtain a statistical average of the distribution, a series of at least 10 photographs of each specimen were taken; each measurement included more than 1000 particles. The secondary phases, such as the Mg_2Si and Al_2Cu particles, and the iron-rich intermetallics were excluded from the measurements and further analysis. Average SDAS values were obtained using the linear intercept method, which involves measuring the distances between secondary dendrite arms along a line normal to the dendrite arms.

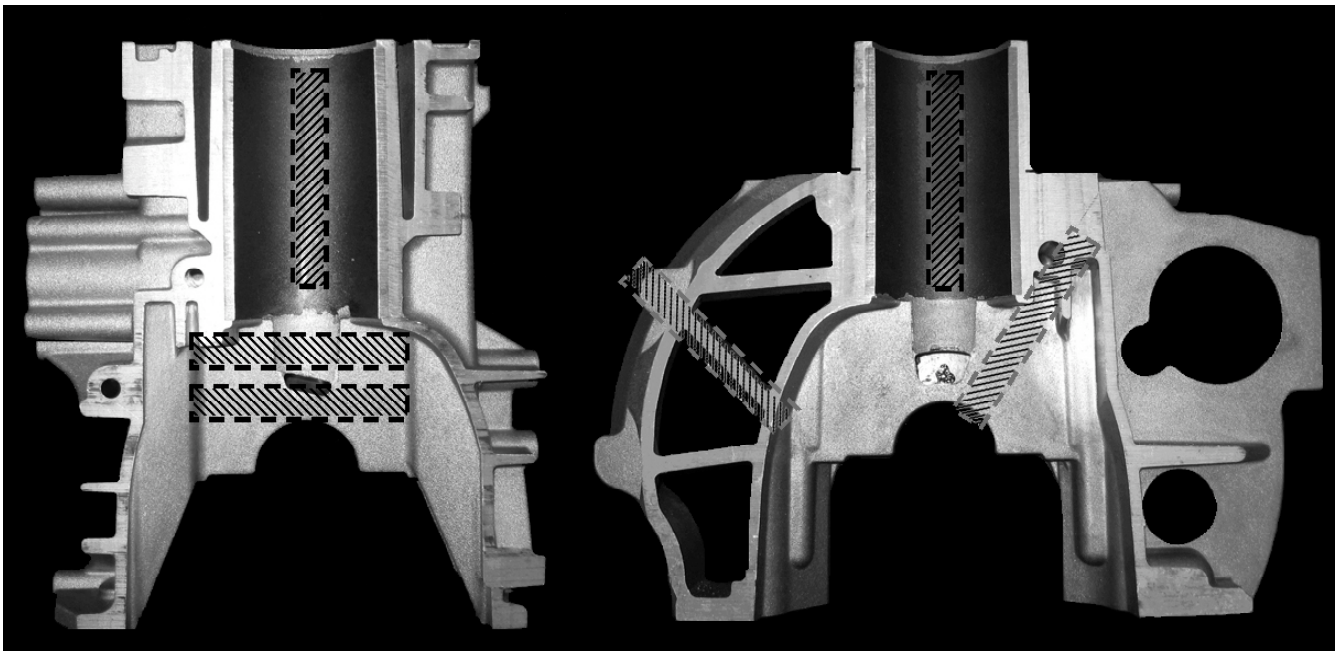

Fig. 2: Position from which tensile specimens were machined.

RESULTS AND DISCUSSION

RADIOGRAPHIC INSPECTION

The results of radiographic investigation show a good integrity of the castings and the absence of defects/porosities with critical size for mechanical properties. This was assured by the vacuum system reducing the gas quantity and, therefore the gas entrapment within the die. However, a small quantity of macroporosity is mostly detected in circular sections or profiles, as well as, in correspondence of the bulkhead supports and underneath liners, especially close to the vacuum line (Figure 3). The defects seem to result from local die filling conditions, which promote the entrapment and dragging of air bubbles.

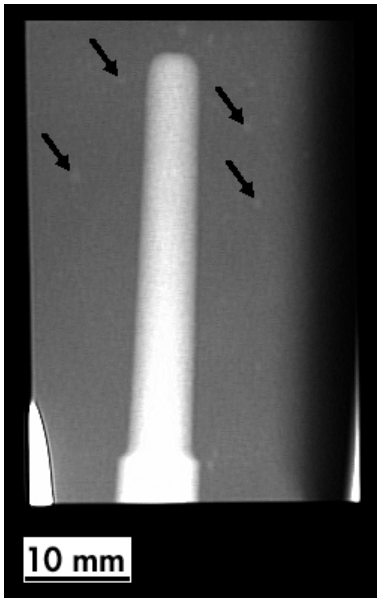

Fig. 3: Radiographic image of the bulkhead support showing the presence of porosity.

MICROSTRUCTURAL OBSERVATIONS

The microstructure consists of a primary phase, α-Al, solid solution, and an eutectic mixture of aluminium and silicon. Al_2Cu secondary phase and Fe-bearing intermetallic are also observed. Differences in solidification between wall and centre of sections reflect upon dimension and distribution of α-Al phase as well as morphology and distribution of eutectic Si particles (Figure 4).

It is noted that the amount of α-Al phase decreases from the wall to the centre line of the sections. As regards the morphology of the α-Al phase, it shows mainly an equiaxed globular-geometry in wall regions and thin wall thickness area. The α-Al cells are little branching due to an increased undercooling governing the entire solidification process and due to the shift in the equilibrium diagram to lower temperatures [23]. The dimensions of α-Al globules increase from the wall to the centre due to lower solidification rates; here, a clear dendrite morphology is observed.

Figure 5 shows the effect of the solidification rate on the dimension and the morphology of eutectic Si particles. Along the wall and in the thin sections, the nucleation prevails on growing mechanism due to an elevated undercooling; therefore, the formation of a fine and fibrous eutectic silicon is promoted (Figure 5a). On the other hand, the eutectic Si particles shows a typical coarse plate-like morphology in centre of thick sections, typical of un-modified aluminium alloys (Figure 5b).

This is supported by quantitative measurements of eutectic particle size, in terms of equivalent circle diameter d, and aspect ratio, α. The results are shown in Figure 6 where the mean value of d and α are plotted as function of SDAS. The effect of increasing cooling rate (i.e. the decrease of SDAS) upon the equivalent diameter is quite pronounced: decreasing dimension of dendrite cell size, equivalent diameter varies from 3.1 to 2.4 μm with a linear tendency. Decreasing SDAS from 20 to 8 μm, the aspect ratio of eutectic Si particles also reduces from ~3 to ~2.2.

In Figure 7, Al_2Cu secondary phase and iron-bearing intermetallics can be also seen. Al_2Cu phase occurs in the form of both pockets of fine eutectic (Al + Al_2Cu) in the interdendritic regions and block-like Al_2Cu particles. The former is due to high cooling rate while the latter is consequence of high fraction of Fe-rich intermetallics, nucleating site for Al_2Cu and resulting from low cooling rate. Fe-rich particles are mainly present in the form of fine blocky-like α-Al(Mn,Fe,Cr)Si particles even if acicular β-Al_5FeSi particles are shown in the thickest sections. The form depends upon the combination of Mn and Cr content and the undercooling degree. High cooling rate promotes nucleation of α-phase, while β-phase formation results from low

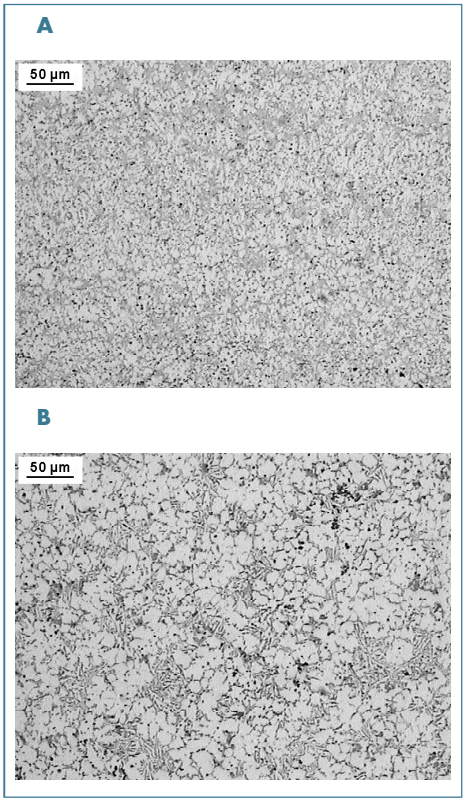

Fig. 4: Microstructure in correspondence of a thick section. It can be noted the changes in the microstructure moving from (a) the wall to (b) the centre of the specimen.

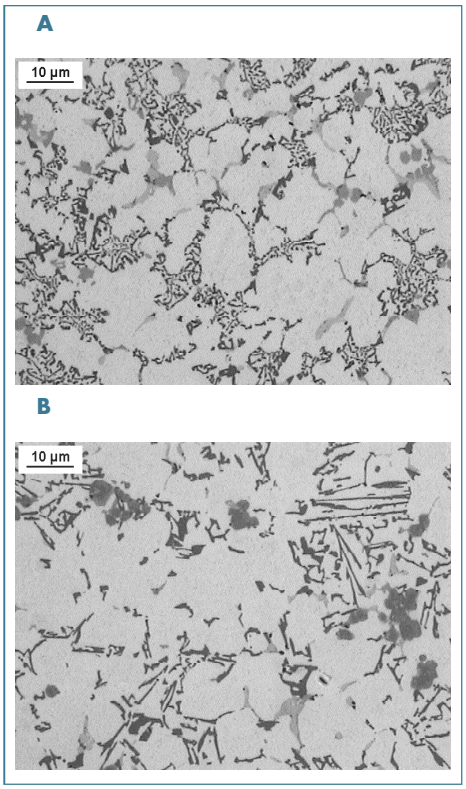

Fig. 5: Eutectic silicon particles with (a) fibrous and (b) lamellar shape in the zones with high and low cooling rates respectively.

solidification rate [21]. Large blocky-like α-Al(Mn,Fe,Cr)Si particles are also observed in the microstructure (Figure 7). In high silicon alloys, α-Al(Mn,Fe,Cr)Si may be primary, and since its crystals tend to be limited by the (111) faces, it appears as more or less well-formed hexagons [24]. These primary phases or complex intermetallic compounds formed with iron, manganese, and chromium are usually called "sludge".

The different microstructure as function of the distance from the wall reflects upon mechanical properties. It is expected that high properties are associated to a finer microstructure as result of a reduced tension filed around the eutectic Si and Fe-rich particles. A quantitative evaluation of this variation is provided in Figure 8, where the Vickers micro-hardness is plotted as function of increasing distance from the wall. The skin layer is in the range of 250-500 mm width, while the hardness decreases from 100 to 85 HV by increasing the distance from the edge.

Common defects of HPDC process, such us oxide films, oxide inclusions, cold shots are observed within the casting, especially in underneath liners and in bulkhead supports close to the vacuum line. Some examples are given in Figure 9.

Segregation bands were detected in the interface between the aluminium alloy and the cast iron liners, as shown in Figure 10. The formation of segregation bands is due to the local collapse of the dendrite network that causes flow of enriched liquid in that zone. The main factors affecting this mechanism are the heat transfer coefficient, the interior flow velocity and the reduced solidification rate. In location of cast iron liners, due to their thin thickness (~5 mm), an equilibrium temperature between liquid alloy and liner is rapidly reached resulting in a lower heat transfer. Thus, the increased solidification time promotes the collapse of α-Al dendrites and, in turn, the formation of segregation [25].

In general, a fine microstructure with small α-Al globules, fibrous eutectic Si and blocky-like Fe intermetallic particle is observed in the top part of the engine blocks as consequence of thin sections resulting in high cooling rate. On the other hand, the bottom part (i.e. bulkhead supports) shows a coarser microstructure and defects due to filling process and lower solidification rate.

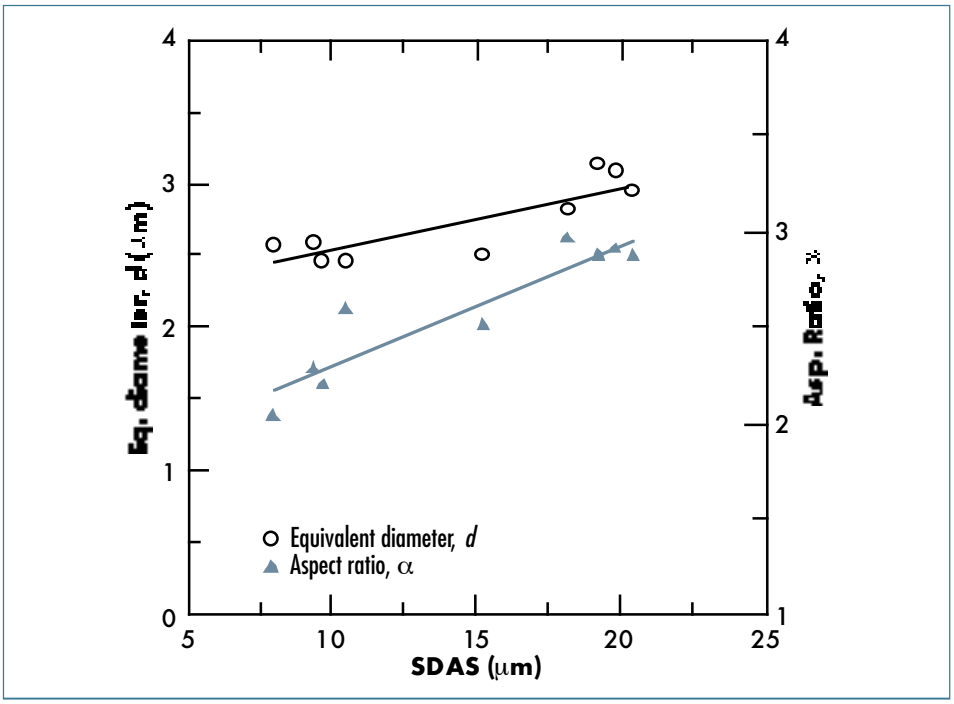

Fig. 6: Average diameter and aspect ratio of the eutectic Si particles as a function of SDAS.

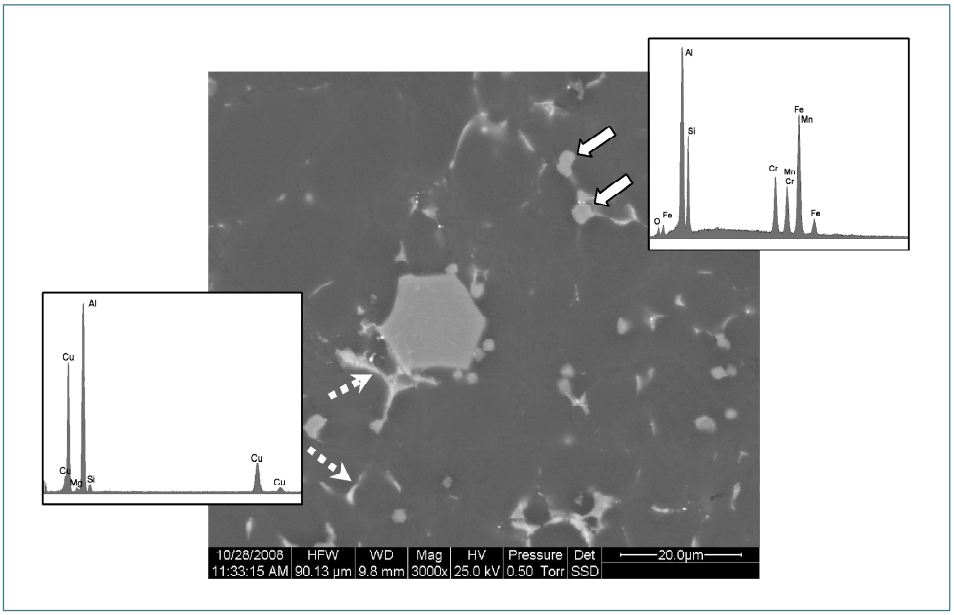

Fig. 7: Microstructure of die-cast $AlSi_9Cu_3$ engine block. Dashed arrows indicate Al_2Cu particles while solid arrows show α-Al(Mn,Fe,Cr)Si intermetallic particles, as revealed by EDS spectra.

TENSILE TESTING

Mechanical properties have been measured in different zones of the engine block. In general, the component shows high mechanical properties suggesting an appropriate setting up of the process parameter that limits the formation of defects.

No sensible variations in the YS values have been obtained; a mean value of 169±8 MPa is measured considering all tensile specimens. This tendency suggests that the effect of the dimension and morphology of α-Al phase and eutectic Si particles is negligible. The best

mechanical properties are measured in the regions between cast iron liners. In this case, the mean values and standard deviation of UTS and elongation to fracture are 274±10MPa and 2.5±0.4% respectively. Conversely, the zones underneath the liners and bulk-head support show an average value of 236 MPa as UTS and of 1.4% as elongation to fracture. Lower values are the consequence of thicker sections along with higher quantity of defects decreasing the mechanical strength of the alloy.

The best UTS and S_f values have been correlate to the microstructure in order to estimate the influence of α-Al phase and Si particle on the fracture behaviour of the alloy. Figures 11 and 12 show a general decrease in UTS and sf values with increasing SDAS or eutectic Si size. An increased dimension of SDAS, from 8 to 20 mm, leads to a reduction of 24% and 70% of UTS and elongation to fracture, respectively. While the decrease of UTS is linear with increasing SDAS values, the elongation to fracture decreases exponentially. The type of correlation has been selected on the base of the highest value of the coefficient of determination R^2 measured for different regression functions. The coefficient R^2 measures the quality of the least-squares fitting to the original data and it can be written as follows:

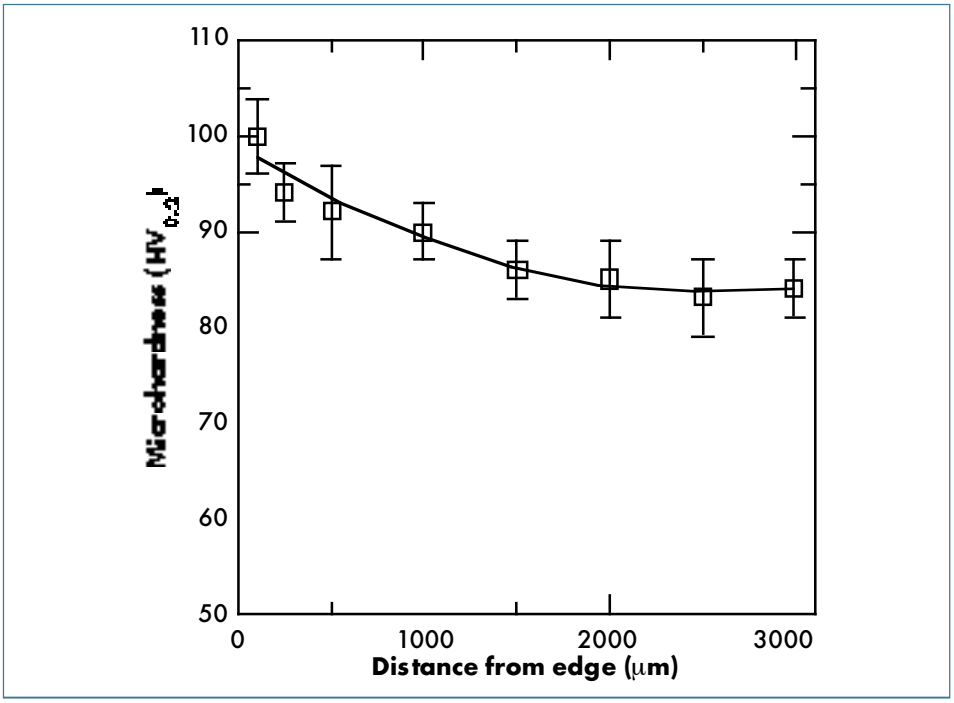

Fig. 8: Vickers microharness measured along the cross section of a specimen. Standard deviations are given as error bars.

$$R^2 = 1 - \frac{\sum_{i=1}^{n} (f(x_i) - g(x_i))^2}{\sum_{i=1}^{n} (f(x_i) - \bar{f}(x_i))^2} \qquad (1)$$

where x_i is the discrete variable, $g(x_i)$ is the corresponding calculated value using the regression function, $f(x_i)$ is the corresponding experimentally measured value, $\bar{f}(x_i)$ is the

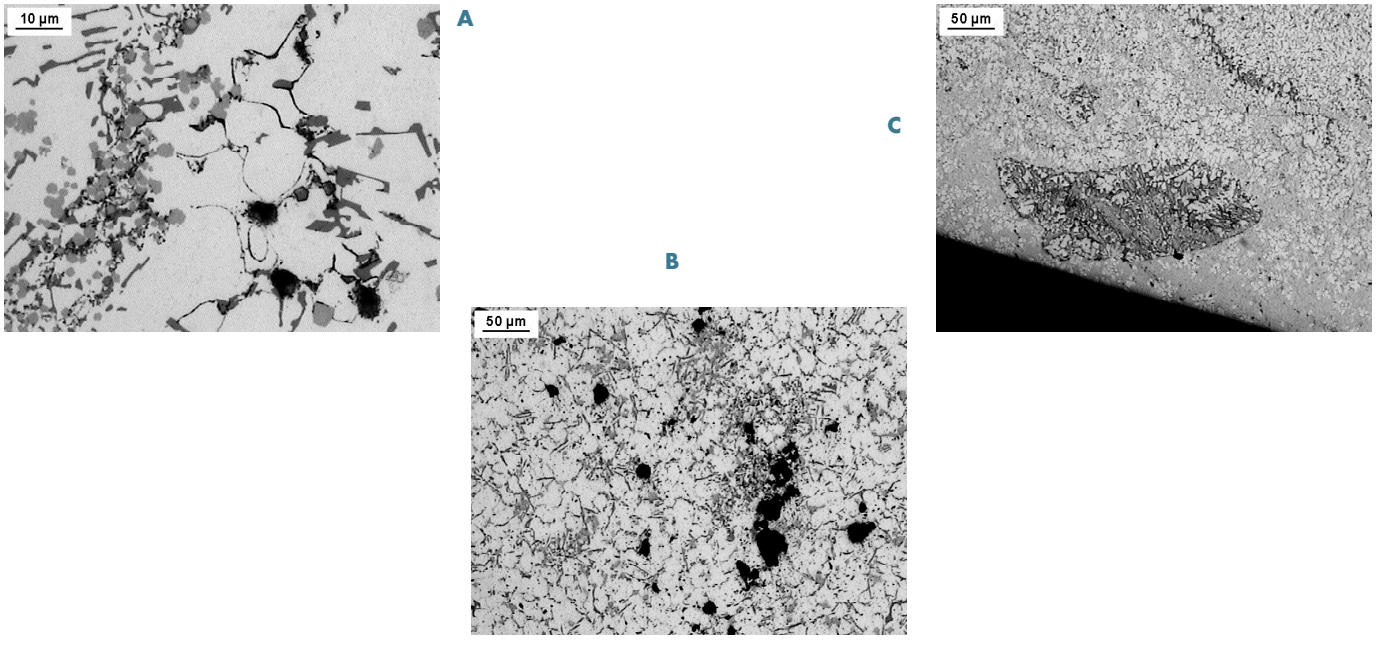

Fig. 9: (a) Oxide inclusions and films, (b) porosities and (c) cold shots observed in diecastings.

mean value of experimental data and n is the total number of experimental points. When $R^2 = 1$, the fit is perfect.

For both functions describing the dependence of UTS and elongation to fracture on SDAS, the calculated R^2 is 0.52. The fairly good value of R^2 is consequence of the scatter in experimental data related to the defects which are intrinsic in a HPDC component and, thus, difficult to be completely isolated.

A reduction of the mechanical properties is also observed when the size of eutectic Si particles increases (Figures 12). The UTS varies from 281 to 219 MPa and the elongation to fracture decreases from 2.9% to 0.8%. By increasing the solidification time, coarser Si particles can be observed in the microstructure leading to high tension field around particles. This promotes cleavage mechanism and, thus, fracture can easily propagate. The best fitting lines are similar to that of Figure 11: a linear function with R^2=0.83 and an exponential function with R^2=0.89 describe the variation of UTS and S_f on eutectic Si particles, respectively. This definitively suggests that the elongation to fracture is more sensitive to eutectic Si and SDAS values than the UTS.

Since the plastic behaviour of cast aluminium alloy is influenced by α-Al phase and eutectic Si particles, it is reasonable to expect that the UTS and the elongation to fracture are controlled by a combined effect of SDAS and eutectic Si features. Figure 13 plots UTS and elongation to fracture as function of the product of SDAS, equivalent diameter and aspect ratio of eutectic Si particles. An increased value of this product reflects upon a reduction of UTS and S_f values. It can be observed that

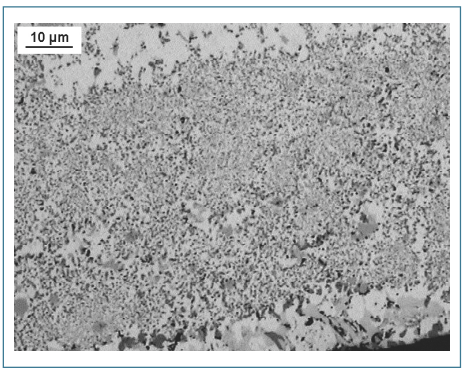

Fig. 10: Segregation bands of eutectic silicon in regions with low solidification rate.

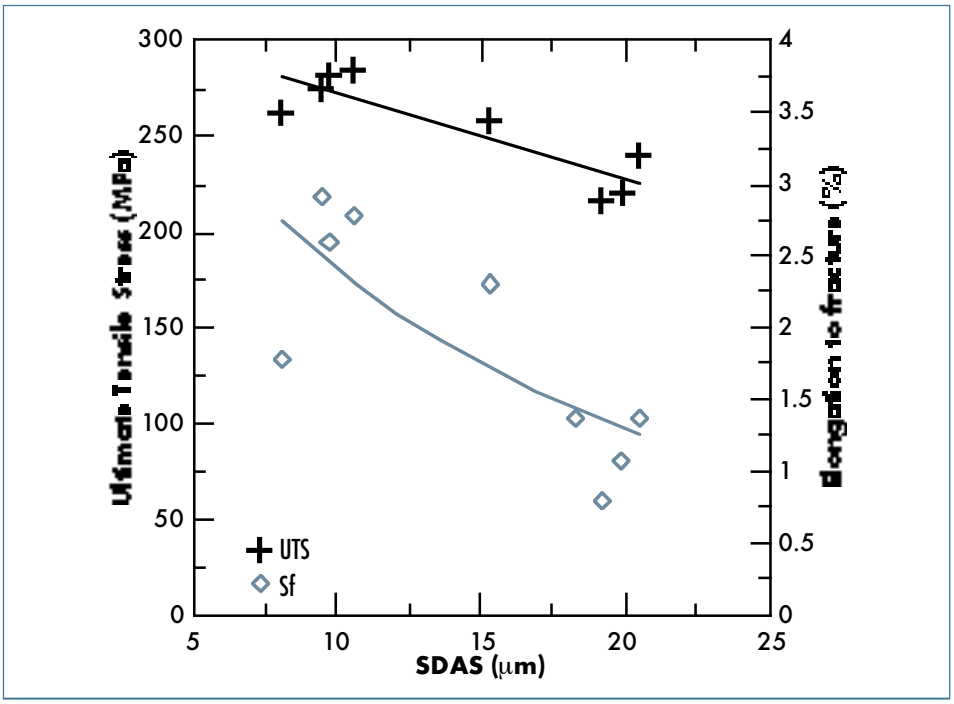

Fig. 11: UTS and elongation to fracture as function of SDAS.

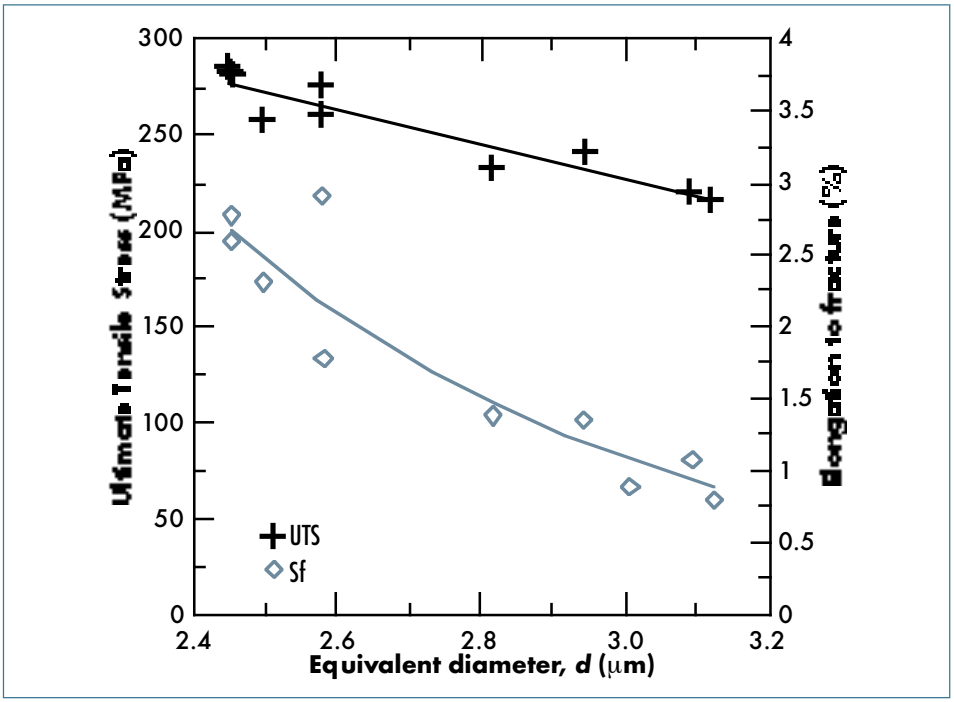

Fig. 12: UTS and elongation to fracture as function of equivalent diameter of the eutectic Si particles.

both UTS and elongation to fracture maintain the tendency shown in the previous plots. The UTS decreases linearly (R^2=0.50) with the product, while the elongation to fracture exponentially (R^2=0.55), mainly for the effect of size and morphology of Si particles.

CONCLUSIONS

Microstructure and mechanical properties of a HPDC 4-cylinders-in-line cylinder block have been analyzed. Based on the results obtained in the present study, the following conclusions can be drawn.

1. A fine microstructure is associated to high solidification rates in correspondence of casting wall and thin sections.
2. Higher solidification time leads to coarser microstructure, formed by large SDAS, eutectic Si particles with coarse plate-like morphology, as well as, higher fraction of blocky-like α-Al(Mn,Fe,Cr)Si phase.
3. In general, a low quantity of defects is detected within the castings. A small quantity of macroporosity are mostly detected in correspondence of the bulkhead supports and underneath liners, especially close to the vacuum line.
4. Mechanical properties are affected by microstructure. The best values of UTS and elongation to fracture are obtained for low SDAS values and small and more compact eutectic Si particles.
5. A coarser microstructure along with higher defect amount decreased the alloy strength, promoting fracture nucleation and propagation.
6. If the combined effect of α-Al and eutectic Si is taken into account, a linear correlation between UTS and product of SDAS, equivalent diameter and aspect ratio of Si particles can be observed; while the elongation to fracture shows an exponential trend, suggesting an high sensitivity on microstructural variation.

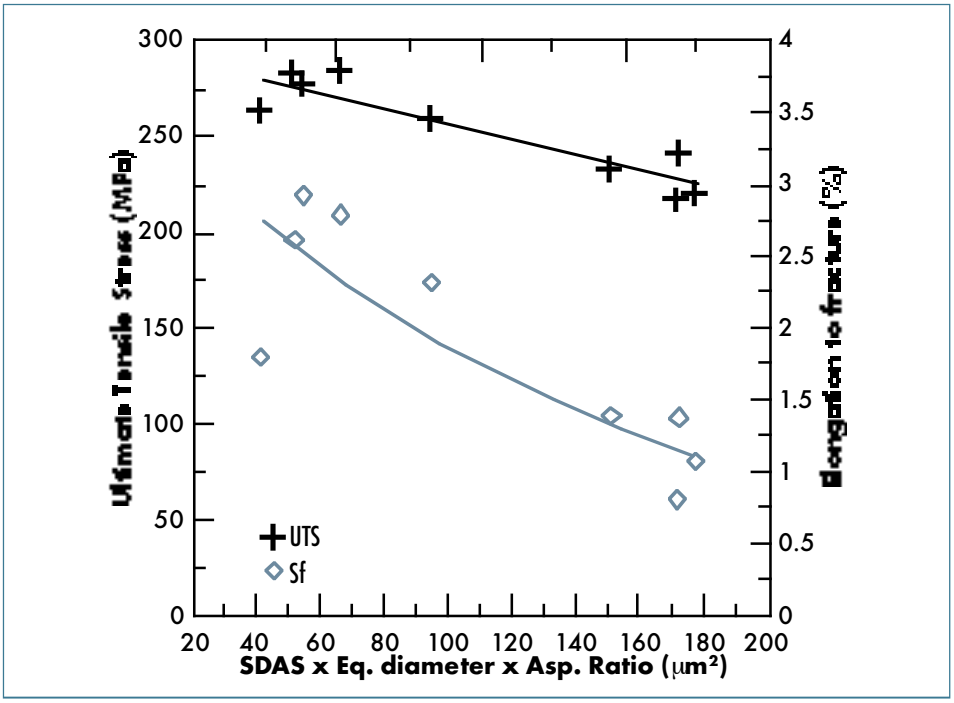

Fig. 13: UTS and elongation values as function of the combined parameter SDAS x Equivalent diameter x Aspect ratio of eutectic Si particles.

ACKNOWLEDGEMENTS

The European Project Nadia- New Automotive components Designed for and manufactured by Intelligent processing of light Alloys (NMP-2004-SME 3.4.4.5, contract n.026563-2) is gratefully acknowledged for financial support.

REFERENCES

[1] Colás, R., A. Rodríguez, J. Talamantes, and S. Valtierra. Solidification analysis of aluminium engine block. Int. J. Cast Metals Res., 17 (2004), 332-338.

[2] Verran,G.O., R.P.K. Mendes and M.A. Rossi. Influence of injection parameters on defects formation in die casting Al12Si1,3Cu alloy: experimental results and numeric simulation. J. Mater. Process Technol., 179 (2006), 190–195.

[3] Avalle, M., G. Bellingardi, M.P. Cavatorta and R. Doglione. Casting defects and fatigue strength of a die cast aluminium alloy: a comparison between standard specimens and production components. Int. J. Fatigue 24 (2002), 1-9.

[4] Timelli, G. and F. Bonollo. Quality mapping of aluminium alloy diecastings. Metal. Sci. Tech., 26 (2008), 2-8.

[5] Shabestari, S.G. and F. Shari. Influence of modification, solidification conditions and heat treatment on the microstructure and mechanical properties of A356 aluminum alloy. J. Mater. Sci., 39 (2004), 2023-2032.

[6] Viswanathan, S., A.J. Duncan, S.A. Sabau, Q. Han, W.D. Porter and B.W. Riemer. Modeling of Solidification and Porosity in Aluminum Alloy Castings. AFS Transactions, 98-103 (1998), 411-417.

[7] Rontó, V. and A. Roósz. The effect of the cooling rate or the local solidification time and composition on the secondary dendrite arm spacing during solidification Part II: Al-Mg-Si alloys. Int. J. Cast Metals Res., 13 (2001), 337-342.

[8] Grosselle, F., G. Timelli, F. Bonollo, A. Tiziani and E. Della Corte. Correlation between microstructure and mechanical properties of Al-Si cast alloys. Metall. Ital., 6 (2009), 25-32.

[9] Chen, Z.W. Skin solidification during

high pressure die casting of Al-$_{11}$Si-$_2$Cu-1Fe alloy. Mater. Sci. Eng., A348 (2003), 145-153.

[10] Ye, H. An overview of the development of Al-Si alloy based material for engine applications. J. Mater. Eng. Perf., 12(3) (2003), 288-297.

[11] Samuel, F.H., A.M. Samuel and H.W. Doty. Factors controlling the type and morphology of Cu-containing phases in 319 Al alloy. AFS Trans., 104 (1996), 893-901.

[12] Niu, X.P, B.H. Hu and S.W. Hao. Effect of iron on the microstructure and mechanical properties of Al die-casting alloys. J. Mater. Sci. Letters, 17 (1998), 1727-1729

[13] Wang, Q.G. and C.H. Cáceres. Fracture mode in Al-Si-Mg casting alloys. Mater. Sci. Eng, A241 (1998), 72-82

[14] Wang, Q.G., C.H. Cáceres and J.R. Griffiths. Damage by eutectic particle cracking in aluminum casting alloys A356/357. Metall. Mater. Trans. A, 34 (2003), 2901-2912

[15] Cáceres, C.H. and J.R. Griffiths. Damage by the cracking of silicon particles in an Al-7Si- 0.4Mg casting alloy. Acta Mater. 44 (1996), 25-33.

[16] Cáceres, C.H. and B.I. Selling. Casting defects and the tensile properties of an Al-Si-Mg alloy. Mater. Sci. Eng., A220 (1996), 109-116.

[17] Gokhale, A.M. and G.R. Patel. Origins of Variability in the fracture related mechanical properties of a tilt-pour-permanent-mold cast Al-alloy. Scripta Mater., 52 (2004), 237-241.

[18] Shankar, S. and D. Apelian. Die soldering: Mechanism of the interface reaction between molten aluminum alloy and tool steel. Mater. Trans., 33B (2002), 465–476.

[19] Jorstad, J.L. Understanding "Sludge". Die Casting Eng., November/December (1986), 30- 36.

[20] Ghomashchi, M.R. Intermetallic compounds in an Al-Si Alloy used in high pressure diecasting. Z. Metallkunde, 78 (1987), 784–787.

[21] Seifeddine, S., T. Sjögren and I.L. Svensson. Variations in microstructure and mechanical properties of cast aluminium EN AC 43100 alloy. Proc. High Tech Die Casting, AIM, (2006), Vicenza.

[22] Zovi, A. and F. Casarotto. Silafont-36, the low iron ductile die casting alloy development and applications. Metall. Ital. 6 (2007), vol.,33–38.

[23] Asensio-Lozano, J. and B. Suárez-Peña. Microstructure-properties correlation of pressure die cast eutectic aluminum-silicon alloys for escalator steps (Part I). Mater. Characterization, 56 (2006), 169-177.

[24] Mondolfo, L.F. Manganese in Aluminum Alloys. The Manganese Center, (1978).

[25] Mo, A., M. M'Handi and H.I. Laukly. Modelling defect bend formation in Al-Si die casting. Proc. High Tech Die Casting, AIM, (2006), Vicenza.